Effects of Stopper Rod Movement on Mold Fluid Flow at ArcelorMittal Dofasco's No. 1 Continuous Caster

R. Liu[1], J. Sengupta[2], D. Crosbie[2], M.M. Yavuz[3] and B.G. Thomas[1]

[1] Department of Mechanical Science and Engineering,
University of Illinois at Urbana-Champaign,
1206 West Green Street, Urbana, IL 61801 USA
Tel.: +1-217-333-6919
Email: bgthomas@illinois.edu

[2] ArcelorMittal Global R&D Hamilton, ArcelorMittal Dofasco Inc.
1390 Burlington Street East, Hamilton, Ontario L8N 3J5 CANADA
Tel: +1 905 548 4739
Email: joydeep.sengupta@arcelormittal.com

[3] Former Researcher in ArcelorMittal Global R&D East Chicago,
3001 East Columbus Drive, East Chicago, IN 46312 USA

Key words: sliver defect, CFD, nail dipping, transient flow, entrapment

ABSTRACT

Effects of stopper rod movement on transient flow phenomena in the mold and formation of sliver defects are investigated via plant measurements and numerical simulations. First, sliver locations are correlated with stopper rod position and level fluctuation histories in the mold by analyzing images of slivers and process data recorded at ArcelorMittal Dofasco's No.1 Continuous Caster. Then, 3-D transient CFD models are developed, validated with plant measurements, and applied to simulate transient flow, particle motion, and entrapment phenomena to reveal how level fluctuations arise, and how the slivers may have formed.

INTRODUCTION

The formation of sliver defects and quality of the final steel product are closely related to the transient liquid steel flow in the mold. Excessive liquid steel surface velocity can shear off and entrain liquid slag droplets, leading to the entrapment of inclusions in the solidifying shell and sliver defects in the final products. The release of clogging material from the SEN can send inclusions such as alumina into the mold and also cause meniscus level fluctuations, resulting in sliver formation. Mechanisms for entrainment of mold slag and formation of defects due to fluid flow problems in the mold can be found in previous reviews [1-3].

Transient flow in the SEN and mold has been studied in some previous work, mainly using water models and computational models. Injecting gas into the SEN significantly affects the flow in the mold, so gas-liquid two phase flow in water models and steel caster molds has been simulated. Thomas and Huang[4] developed a 3-D finite difference model of argon-steel two phase transient flow, and studied the transition of flow pattern from initial steady biased flow to steady symmetrical flow in the mold. Simulation results identified large scale vortex shedding phenomena and correlated argon gas injection with meniscus turbulence. They also used this model to study the effects of argon injection on the flow pattern in the mold[5]. Ramírez-López *et al.*[6] simulated water-air turbulent flow structure in a water model at different casting speeds. Chaudhary *et al.*[7] showed in a of study different bottom nozzle designs that steady K-ε simulations could reasonably quantify time-average flow, including average

transient statistics, such as turbulent kinetic energy. Yuan *et al.*[8] combined accurate transient LES simulations and PIV measurements to reveal the transient nature of evolving turbulent flow structures during nominally steady casting conditions. Zhang] *et al.* [9] used a 3-D URANS model in FLUENT to simulate transient flow during hypothetical casting speed changes, and showed the resulting increase in surface velocity variations.

In practice, transient flow in the SEN and mold is strongly affected by the changing SEN flow rate, which is controlled by the stopper rod position. Sudden movements of the stopper rod are known to cause sliver defects. These important transient events have not been quantified and the mechanisms of defect formation are not understood, and, hence, these are the objectives of the current project. This work is part of an ongoing international collaboration between ArcelorMittal and the Continuous Casting Consortium at the University of Illinois at Urbana-Champaign (UIUC CCC). It combines plant measurements and analysis conducted by ArcelorMittal Global R&D Hamilton, Canada at ArcelorMittal Dofasco's No. 1 Continuous Caster (No. 1 CC), water modeling conducted at ArcelorMittal Global R&D, East Chicago, USA, and computational modeling conducted at the UIUC CCC.

INDUSTRIAL DATA COLLECTION AND CASTER CAMPAIGNS

In the current work, some sliver defects were detected on coils (produced from slabs cast at No. 1 CC) with the aid of downstream feedback from the Automated Surface Intelligence System ("ASIS")[10] and the slivers were removed from the coils in accordance with quality control protocols. Events at No. 1 CC were analyzed and a direct link between transient events in the mold and these slivers was established, and therefore, were chosen to support this study. SEM analysis was performed at ArcelorMittal Global R&D Hamilton to identify the composition of the entrapped particles located inside the sliver samples. The formation locations on slabs were calculated from the entrapment depths in the coil, knowing the defect locations along the coil length and the thickness reduction ratios between the coils and slabs. Data was further analyzed to estimate the entrapment locations below the meniscus and along the vertical distance of the mold. The time of particle entrapment was also calculated using the casting speed.

An example of one such sliver-causing event was found to be due to an abrupt movement of the stopper rod. An SEM image of the sliver defect obtained from the coil sample is pictured in Fig. 1, and had a composition indicating it was captured mold flux. This particular defect was correlated to a shell thickness of 3.2mm in the 218mm-thick slab where it got entrapped. This suggests formation in the mold, 27mm below the meniscus. The history of important casting conditions including stopper rod movement, casting speed changes, and level fluctuation signals were collected from corporate database. The normalized curves are shown in Fig. 2, with the conditions of mold level and stopper rod position at defect formation time defined as unity. A sudden stopper movement is evident in the figure and this event was chosen as a test case for development of the computational modeling procedure of this project.

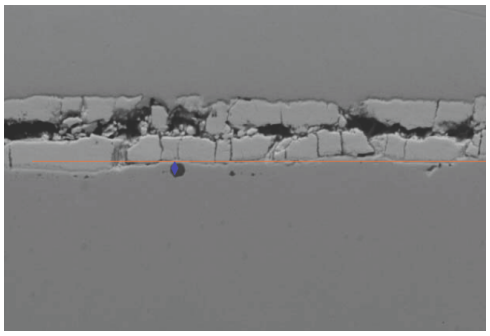

Figure 1. Sliver SEM Micrograph from a coil sample chosen for this study

COMPUTATIONAL MODELS

A system of computational models is being developed to investigate defect-causing events such as described in the previous section. First, 3-D CFD models were developed for the caster of interest and validated using both water model experiments and nail dipping tests from plant trials. Next, a new model to estimate the real history of the steel flow rate through the SEN was

developed to correlate the stopper rod position, casting speed, and surface level histories. This predicted flow rate is adopted as the inlet boundary condition for the validated CFD model. The transient CFD model is initialized with a simulation of nominal steady-state conditions. Fluid properties used in the simulations are given in Table I. Finally, a transient argon-steel two phase flow simulation was performed to simulate the stopper rod movement as described previously.

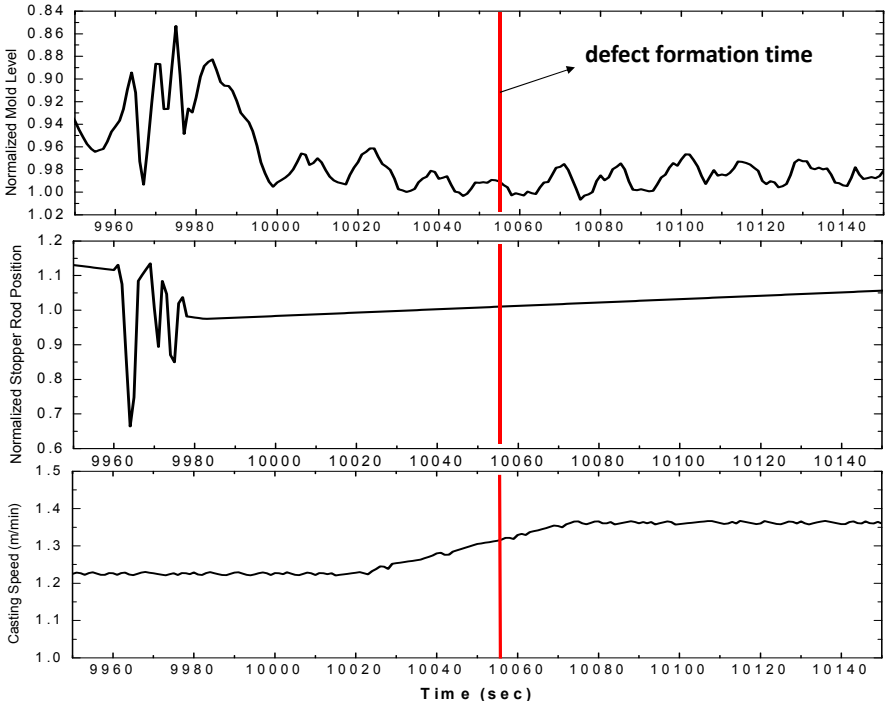

Figure 2. Mold level signal, stopper rod position and casting speed history during entrapment event

Table I. Fluid properties

	Water	Air	Steel	Argon (at 1832 K)
Density (kg/m^3)	998.2	1.225	7200	0.291
Viscosity (Pa*s)	0.001	1.79 x 10^{-5}	0.0056	8.18 x 10^{-5}

VALIDATION WITH WATER MODEL EXPERIMENTS

Water model experiments including the gas injection were conducted at ArcelorMittal Global R&D for the two cases in Table II. The reduced-scale water model of the No. 1 CC was used in the experiments with a bifurcated SEN submerged at a depth of 76mm below meniscus. Instrumentation installed at the facility was used to measure surface velocity midway between the SEN and narrow face. The equivalent full-scale caster dimensions were 1600mm wide and 225mm thick. Further details of the water model are provided elsewhere[11]. 3-D model simulations were conducted for these 2 cases using the quarter-mold geometry and mesh shown in Fig. 3. The continuity and Reynolds-Averaged Navier-Stokes (RANS) equations with the standard K-ε turbulence model were discretized with first-order upwinding finite-volume method, and solved using FLUENT. Wall boundaries utilized the Enhanced Wall Treatment (EWT).

Table II. Water model simulation cases (converted to equivalent full scale caster)

CFD Cases	SEN Depth (mm)	Casting Speed(m/min)	Total Gas Flow Rate (SLPM)
Case 1	170	1.5	0
Case 2	170	1.5	8.0

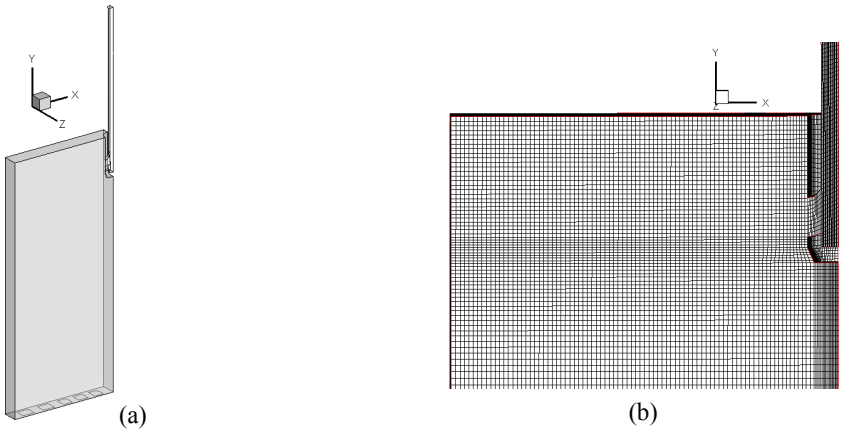

(a) (b)

Figure 3. Quarter water model geometry (a) and mesh (b)

The typical double-roll flow pattern predicted for case 1 is shown in Fig. 4a. The horizontal velocities taken 10 mm below the top surface are shown in Fig. 4b. Error bars indicate velocity fluctuation estimated via local turbulent kinetic energy. The latter predictions are compared with the LDV water measurements, which show an averaged velocity over 20 seconds during the water model experiments. The match observed at the quarter point indicates that the model is reasonably accurate.

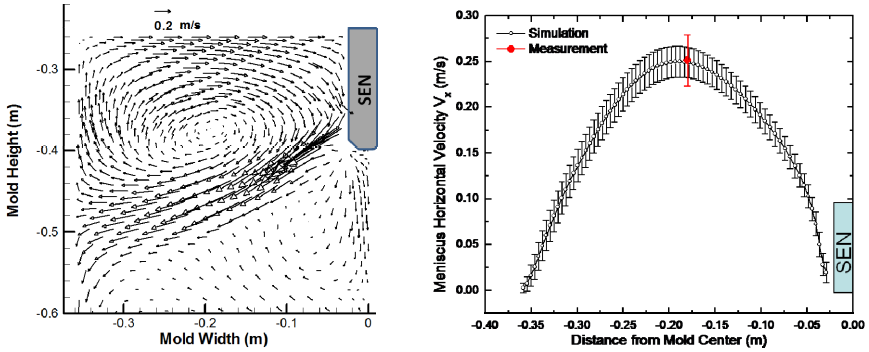

(a) (b)

Figure 4. Single-phase water model flow a) velocity vectors and b) meniscus horizontal velocity profile

For case 2, the mixture model was chosen to solve for the average velocity field, assuming an average bubble size of 2.7 mm according to Bai's model[12, 13]. The water-air two phase flow simulation results in Fig. 5 show that injecting air into the water model causes the water jet to split into two streams at nozzle exit. One leads towards the narrow face wall, as for single-phase flow. The other stream is buoyed upwards towards the top surface due to drag from the rising gas bubbles. Fig. 6 shows how most of the bubbles rise and escape near to the SEN. Higher gas injection rate into the SEN tends to transform the double roll flow pattern into a more complex flow, and eventually into a single-roll flow pattern.

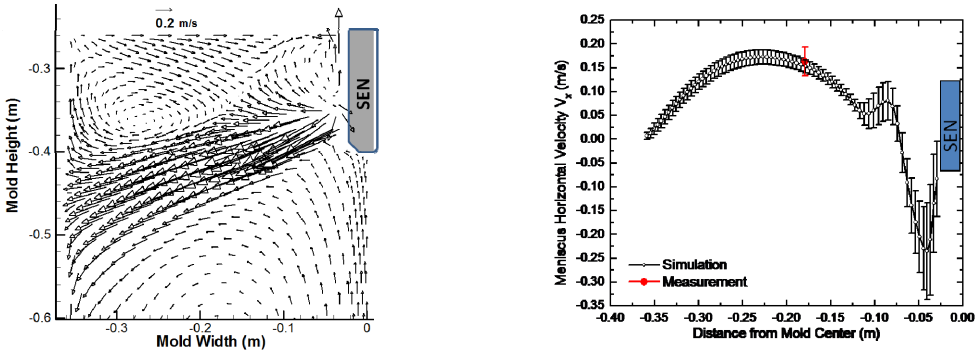

(a) (b)

Figure 5. Water-air-two-phase flow water model a) velocity vectors; b) meniscus horizontal velocity profile

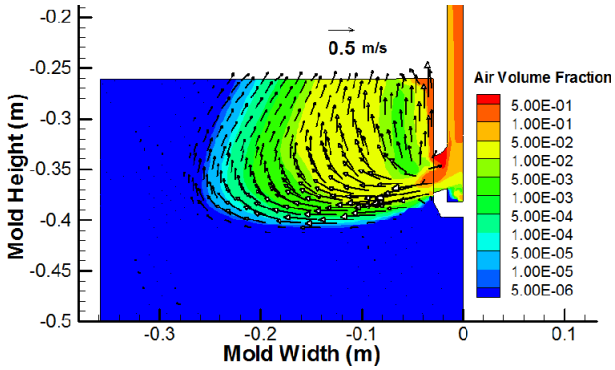

Figure 6. Air velocity and volume fraction distribution

VALIDATION WITH PLANT NAIL DIPPING TESTS

Nail dipping tests were conducted to measure liquid steel surface velocity at Dofasco's No. 1 CC. First, the accuracy of the method was validated by comparison using a separate measurement of surface velocity with a Sub-meniscus Velocity Control (SVC) system. Then, further nail dipping tests were conducted to validate the CFD model predictions of flow in the steel caster.

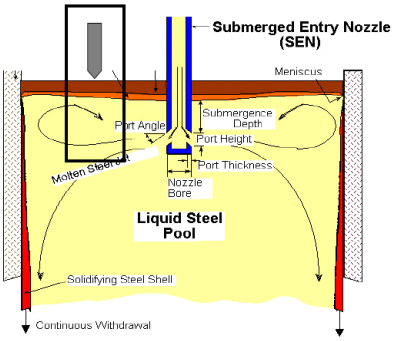

Figure 7. Surface slag layers and CC process[18]

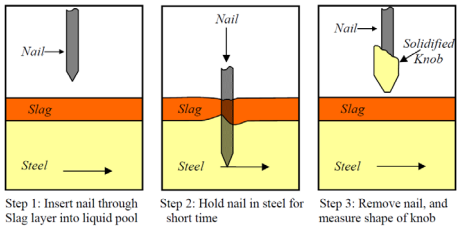

Figure 8. Procedures for nail dipping Test[19]

Nail-Dipping Test Method

The procedure of nail dipping is shown in Figs. 7 and 8. A nail, or board with several nails, is lowered through the slag layer into the top surface of the mold top for 3-5s. The flowing steel is pushed up the slide of nail, leaving a sloped solidified knob or lump upon removal, as shown in Fig. 9. The empirical equation shown in Fig. 10 correlates the lump height difference and lump diameter with the liquid steel surface velocity. This empirical equation was obtained by curve-fitting the simulation results from

Figure 9. Nail and lump[17]

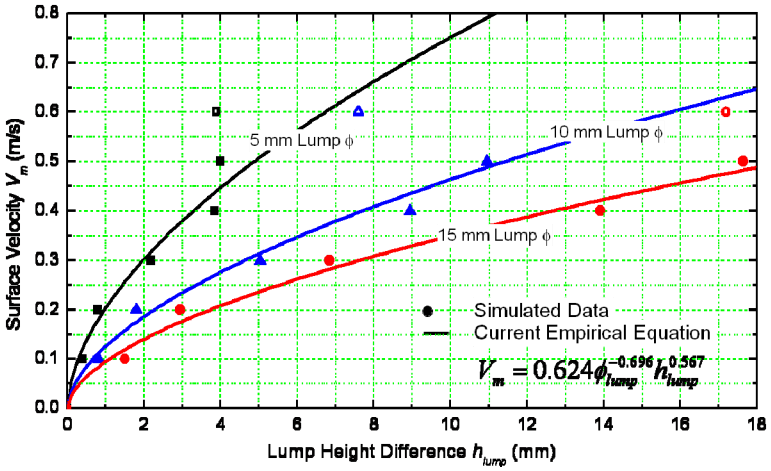

Figure 10. Curves to convert nail lump height difference into velocity magnitude[17]

Rietow and Thomas' model[14, 15]. The nail dipping method was then validated by SVC[16] measurements in an operating commercial caster during a series of casting condition changes[17], as shown in Fig. 11. Both methods were able to track the same history of velocity changes at the surface through a series of changes in operating conditions.

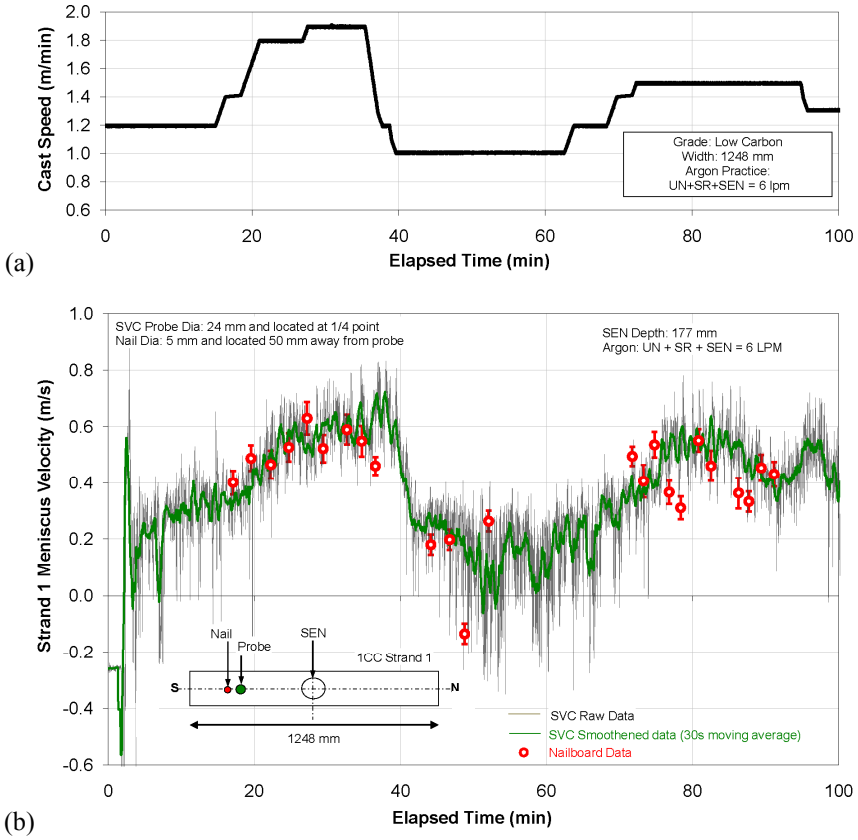

Figure. 11 Plant trial comparing two surface velocity measurement methods[17] .
(a) Casting speed history; (b) Meniscus velocity history from SVC and nail dipping.

CFD Model Validation with Nail-Dipping Measurements

One quarter of the SEN and mold were simulated for the conditions in Table III. Fig. 12 shows the geometry and mesh of ~0.23 million hexahedral structured cells. The Dofasco No. 1 caster was 983mm wide x 225mm thick x 2.5m long with a bifurcated SEN, submerged 186mm below meniscus.

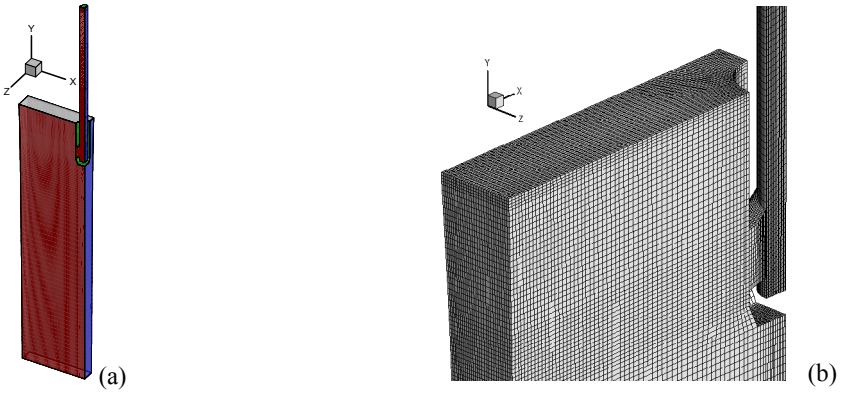

Figure 12. Computational domain geometry and mesh

The numerical surface velocities are compared with results of the nail dipping tests in Fig. 13. A reasonable match is obtained, which tends to validate the model. These results also show that increasing gas volume fraction (by decreasing casting speed), tends to change the double-roll flow pattern into a complex flow pattern, as expected from the water model results.

Table III. Steel caster simulation cases

CFD Model	Casting Speed (m/min)	Total Argon Flow Rate (SLPM)
Case 1	1.5	6.0
Case 2	1.7	6.0
Case 3	1.9	6.0

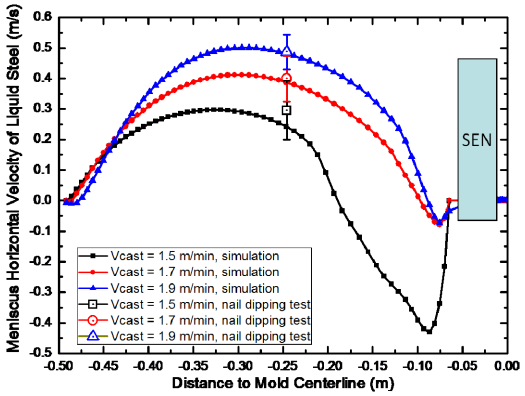

Figure 13. Horizontal liquid steel velocity profile along meniscus centerline

Velocities near the SEN are directed towards the narrow face, in the opposite direction of classic surface velocities from the narrow face. This reverse flow near SEN is caused by the liquid steel dragged to the meniscus by the rising bubbles.

INLET FLOW RATE MODELING

The first step in conducting a transient simulation of defect formation caused by mold flow is to determine how the liquid steel flow rate at the SEN inlet changes with time during the event. In theory, flow rate through the SEN changes directly with stopper rod position, according to the tundish depth. In practice, however, minor changes to the shape of the flow passage near the stopper tip due to clogging or erosion changes the flow resistance dramatically[20]. Thus, modeling must be combined with measurements to determine the flow rate. During this transient event, since casting speed changes, inlet flow rate changes, and mold flow dynamics all contribute to the rise or drop of the meniscus surface level in the mold, the flow rate history cannot be determined simply by any one of the recorded signals. For the transient simulation of this case, two separate models were developed to predict the liquid steel flow rate through the SEN: a stopper-position-based model and a metal-level-based model. The stopper-position-based model is derived from Bernoulli's equation, and calculates flow rate based on the measured stopper rod position. The metal-level-based model conducts a mass balance at the SEN inlet, from the measured meniscus level and casting speed histories.

Stopper-Position-Based Model

Equation (1) gives an expression to calculate inlet SEN flow rate based on stopper rod opening and other parameters.

$$Q_{SEN} = A_{SEN}\sqrt{\frac{2g\left(-h_{sen\_sub}+f_{tundish}h_{tundish}+L_{SEN}\right)}{1+0.5\left(\frac{A_{SEN}}{C_2h_{SRO}^2}\right)^2+\left(\frac{A_{SEN}}{C_2h_{SRO}^2}-1\right)^2+C_1\frac{L_{SEN}}{D_{SEN}}+C_3}} \quad (1)$$

A_{SEN} is the SEN inner bore cross-section area; h_{sen_sub} is the submergence depth of SEN, $h_{tundish}$ is the total height of the tundish; $f_{tundish}$ is the tundish weight fraction; L_{SEN} is the total length of SEN; D_{SEN} is the SEN inner bore diameter; h_{SRO} is the stopper rod opening. The three parameters in the equation, C_1, C_2 and C_3, are adjustable coefficients that represent different pressure losses. C_1 is for friction. C_2 is for the stopper rod gap. C_3 is for clogging. The influence of each of these parameters on the correlation curve

that relates stopper rod position and flow rate is shown in Fig. 14a, 14b and 14c. The important effect of tundish weight fraction is shown in Fig. 14d, relative to 100% full at 1.45m depth.

These figures also include measured flow rates, obtained based on long time periods of steady casting. The predictions span the range of the measurements, suggesting that the model is generally reasonable. However, the scatter suggests simultaneous changes in more than one coefficient, especially clogging condition and tundish level. A sophisticated 3-D CFD model of similar behavior for flow through partially-open slide gates developed by Bai[20] reached similar conclusions. After calibrating this model, the clogging condition can be determined given the measured tundish level, stopper rod position, and steady casting speed. This model is thus a useful tool on its own.

Metal-Level-Based Model

For the metal-level-based model, equation (2) is used to calculate the inlet SEN flow rate based on the measured mold level signal and casting speed.

$$Q_E(i) = \frac{h_m(i+1) - h_m(i-1)}{2\Delta t}\left(W * T - \frac{\pi d_{SEN,outer}^2}{4}\right) + V_{cast}(i) * W * T \tag{2}$$

The index i in this equation represents the current time step; Δt is the time step size, $V_{cast}(i)$ is the casting speed at time step i; W is the mold width, T is the mold thickness; h_m is defined as the meniscus level which is a function of time; $d_{sen,outer}$ is the SEN outer bore diameter.

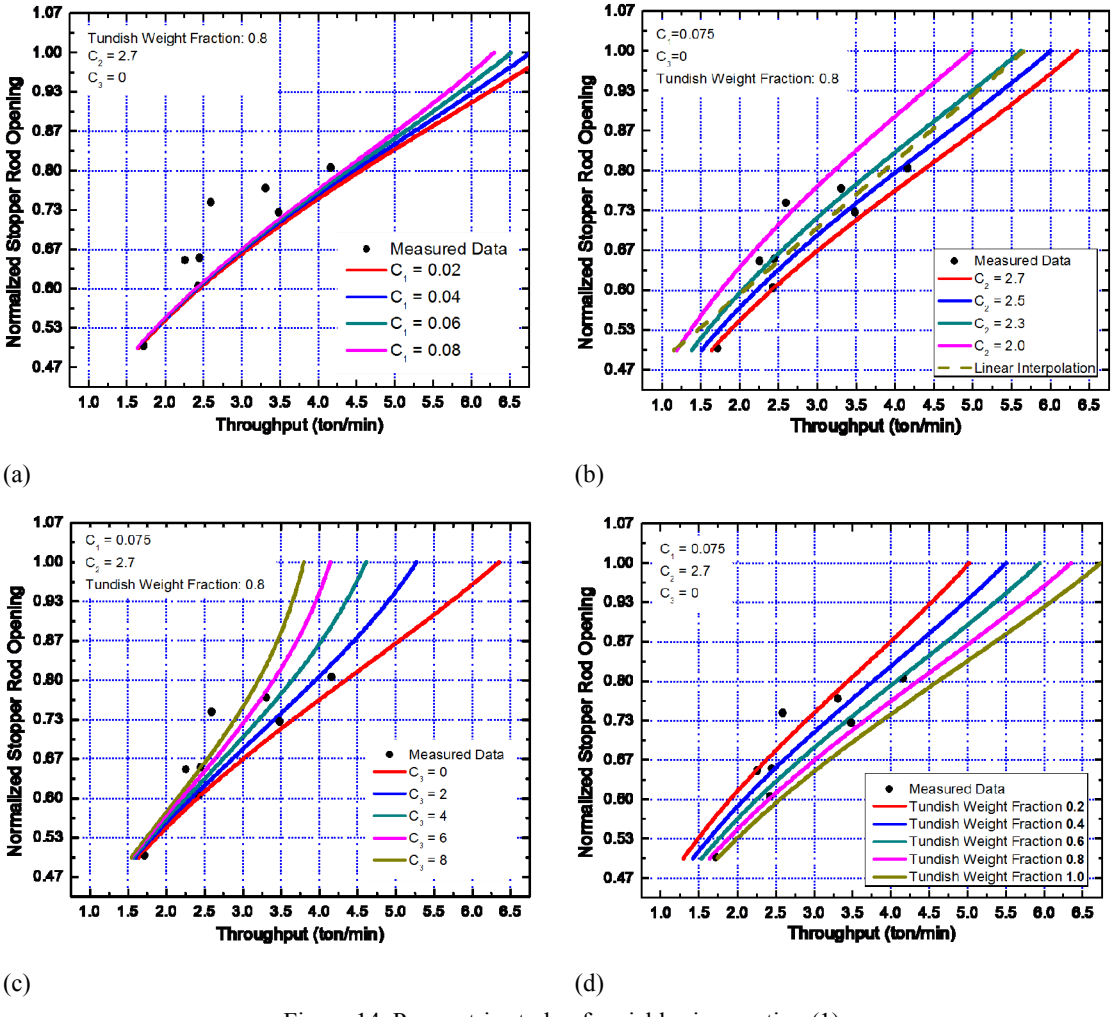

Figure 14. Parametric study of variables in equation (1)

(a) Effect of C_1; (b) Effect of C_2; (c) Effect of C_3; (d) Effect of tundish weight fraction

Calculation of SEN Inlet Flow Rate

Part of the data for the example transient event from Fig. 2 is replotted in Fig. 15. Circles in this figure represent all of the measured casting speed and mold level, as the sampling frequency was 1/s. A cubic spline interpolation was performed to add more data points to smooth the curve for the metal-level-based model (described later). Fig. 15 shows the predicted SEN inlet flow rates changing with time from both the stopper-position-based model and the metal-level-based model. The flat black dashed line reflects that the recorded casting speed was approximately constant throughout the event. However, the predicted flow rates from both models change dramatically with time. Moreover, the predictions from the two models differ greatly, due to neglect of mold flow dynamics. However, if the flow rate curve from the metal-level-based model is translated ahead in time by 1.2 sec, then its peaks and valleys match closely with the stopper-position-based model prediction. This match indicates that it takes about 1.2 sec in this system for a flow rate change at the stopper rod to travel to the meniscus. This time can be regarded as the "response" time for this stopper rod control system.

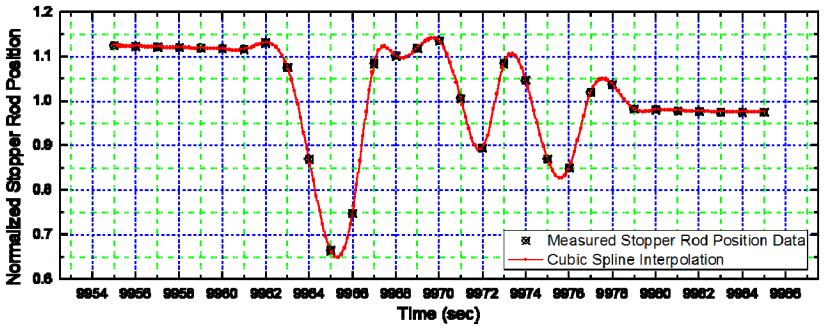

Figure 15. Measured and interpolated normalized stopper rod position (a) and mold level signal (b)

It can be observed in Figs. 2a, 15 and 16 that at ~ 9961 sec, a transient event occurred. A sudden perturbation travelled from the SEN inner bore at this time, which caused the rapid increase in mold level. Then, the stopper rod was closing in ~2s, causing the great decrease in flow rate. At ~9965.3 sec, the liquid steel flow rate reduced to almost 0. However, the metal-level-based model suggests a much higher flow rate of ~1.9 tonne/min at this point. This lack of agreement suggests that the mold level signal, which

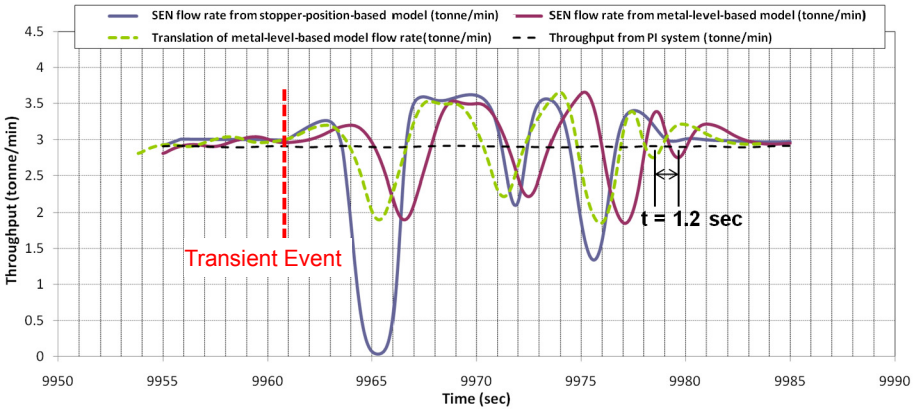

Figure 16. Predicted SEN liquid steel flow rate by stopper-position- and metal-level-based models

is measured only at one point on the top surface, does not represent the true average meniscus level during transient conditions. Thus, to simulate this transient event, the flow rate curve from the stopper-position-based model was converted to velocity as the chosen inlet boundary condition to the SEN.

SIMULATION OF A TRANSIENT EVENT

The unsteady RANS model of turbulent flow in the nozzle and mold was applied to simulate a realistic transient case using the inlet flow-rate history from the stopper-position-based model in Fig. 16 and the full-mold geometry. Fig. 17a displays the blocking strategy for mesh generation and the mesh of 0.8 million structured hexahedral cells that was used in this model. The model geometry of the Dofasco No. 1 caster was 1472mm wide x 225mm thick x 3.0m long with a bifurcated SEN submerged 166mm below meniscus. The argon injection flow rate in this case is 7.5 SLPM.

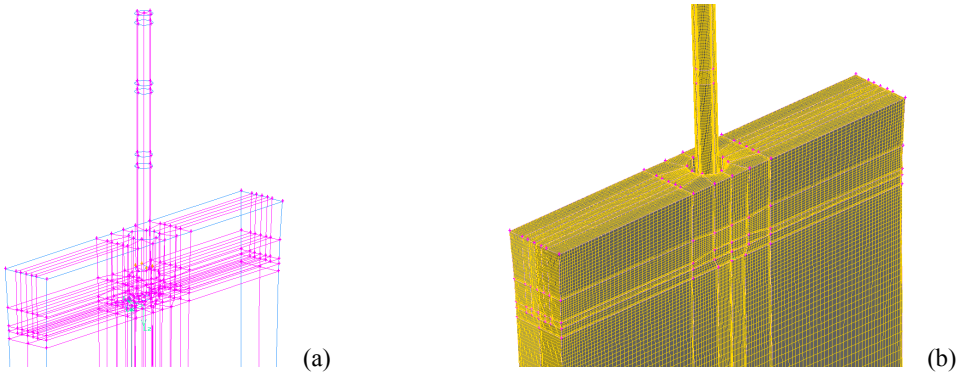

(a) (b)

Figure 17. Geometry (a) and mesh (b) of the CFD model for the transient simulation

The mixture model is used to solve for this argon-steel two phase flow. The standard K-ε model is adopted in current work to handle turbulence of the mixture. For the transient simulation, 0.01 sec is chosen as the time step size. No-slip wall is adopted as the boundary condition at mold top surface, as the sintered slag layer serves as a solid wall. In order to take into account the solidifying shell, mass and momentum sinks[21] are added to the shell boundary cells via user defined function (UDF) in FLUENT. Pressure boundary condition is applied at mold outlet. The bubble size estimated by Bai's model[12, 13] is 2.5 mm, and a mass sink, representing the argon gas flow rate escaping the top surface into the slag layer, is added in all cells next to the top surface.

Fig. 18 shows the quasi-steady liquid steel velocity distribution calculated prior to the transient event. A double-roll flow pattern is observed in Fig. 18a, and the flow pattern on the left and right sides of the mold are symmetrical as required. Fig. 18b shows a

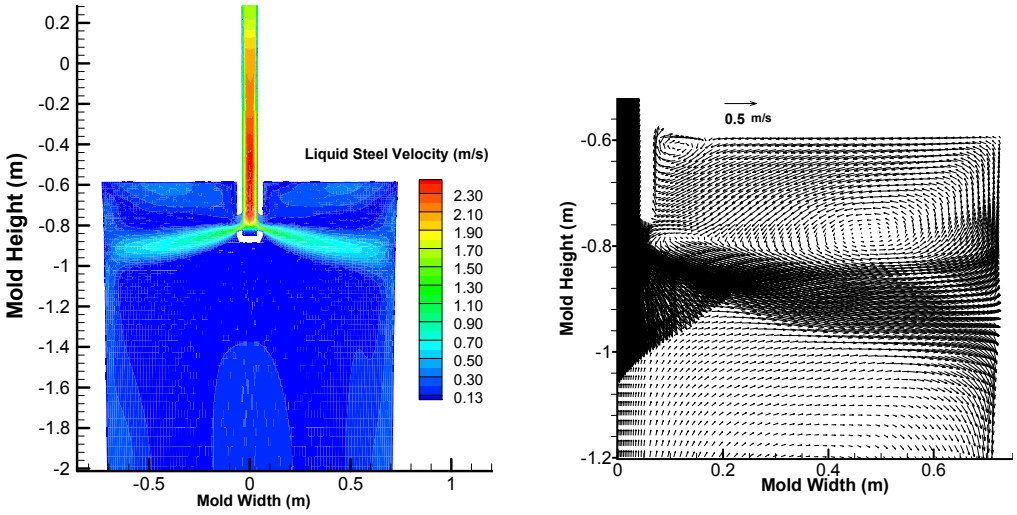

(a) (b)

Figure 18. Quasi-steady state liquid steel velocity field

stream of liquid steel rising along the SEN outer surface toward meniscus. This is due to the upward drag force exerted on the steel stream by rising argon bubbles. Larger bubbles usually gather close to SEN outer wall, and float directly up to the meniscus. A small swirling region is also found at the corner by SEN outer surface and meniscus.

Argon volume fraction is shown in Fig. 19a. The argon bubbles are distributed in a limited space near the SEN in the mold. A gas sheet possibly forms along the SEN inner wall, as indicated by the high argon fraction there. Gas then gathers around the port exit, especially near the port upper edge. Fig. 19b shows the gas velocity distribution at the center plane between broad faces. Gas escapes from top surface between the SEN and quarter point.

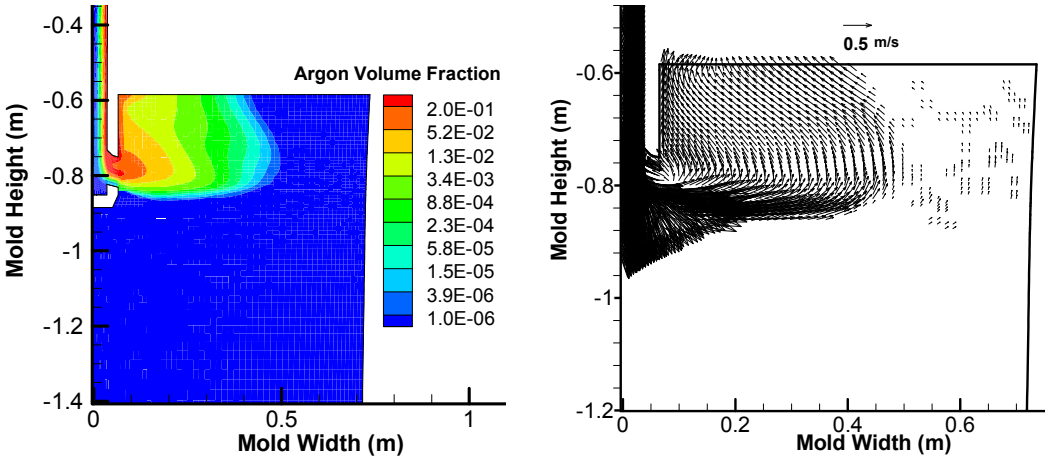

(a) (b)

Figure 19. Quasi-steady state argon volume fraction (a) and velocity distribution (b)

Example snapshots of the evolving flow pattern from ~9963 sec to ~9967 sec during the transient simulation of the transient process are plotted in Fig. 20. Fig. 20a displays a liquid steel velocity field very similar to the one at quasi-steady state shown above. The starting time of 9963.4 sec is reset to 0sec for simplicity. After 1.2s, Fig. 20b shows evidence of the decreasing flow rate at the SEN inlet with the steel jet moving slightly upward as its speed decreases. After 2.2s, Fig. 20c, shows that flow rate decreasing to almost zero, the jet angle leaving the port drops steeper downward,, and naturally decreases speed everywhere in the mold. After that, steel flow rate starts to increase at SEN inlet, and jet penetrates the mold, as shown in Fig. 20d, 20e and 20f. As expected, many more seconds are required before the surface velocity notices the change. Improvement of this simulation using a less diffusive filtered URANS modeled is planned. When combined with further models and analysis of particle capture, these simulations will reveal the likely mechanism(s) of sliver defects, and help in the development of criteria to predict defect formation in realistic plant conditions.

SUMMARY

1. A 3-D transient K-ε model of steel and argon gas fluid flow in the SEN and mold has been developed and compared with water model experiments and nail dipping tests in an operating steel continuous caster. Although it can match the time-average flow patterns, a less diffusive turbulence model is needed to capture all of the small-scale transients.
2. The nail-dipping test has been validated with independent flow velocity measurements in a commercial steel caster and shown to be a simple but powerful method to quantitatively measure surface steel velocities in the mold.
3. A new mathematical model has been developed to quantify the flow rate history through the SEN due to stopper-rod movements, and found to be consistent with plant measurements. These results are needed as inlet boundary condition for future numerical simulations of transient events in the mold.

ACKNOWLEDGEMENTS

The authors would like to thank the members of the Continuous Casting Consortium in University of Illinois at Urbana-Champaign for their support of our research work, and also to S. Chung, M. Trinh and D. Currey at ArcelorMittal Dofasco Inc. in Canada for their help with the plant trials. ArcelorMittal Global R&D in Maizières, France is acknowledged for providing

the SVC devices for trials.

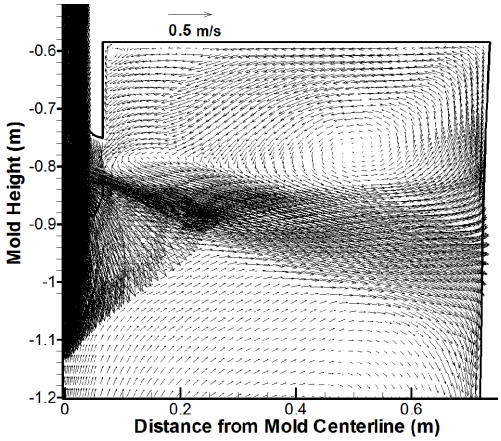

(a) Time = 1sec (9963.4 sec);

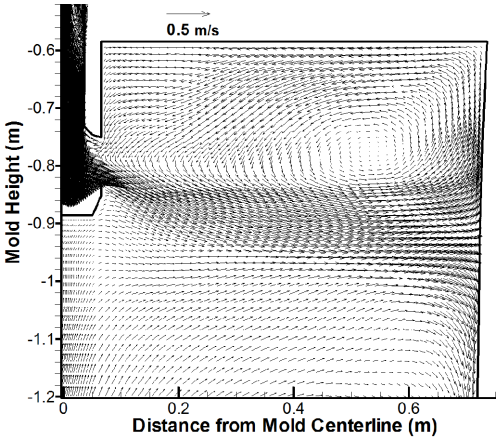

4. Time = 1.2 sec

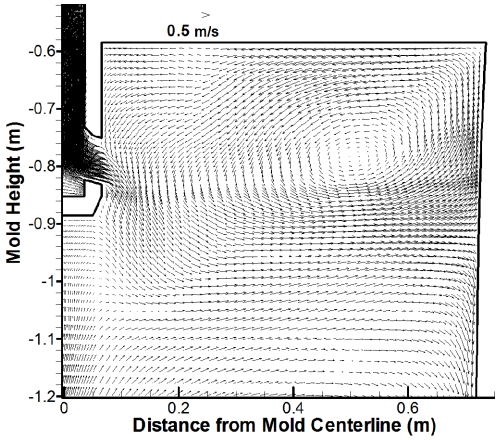

(c) Time = 2.2 sec

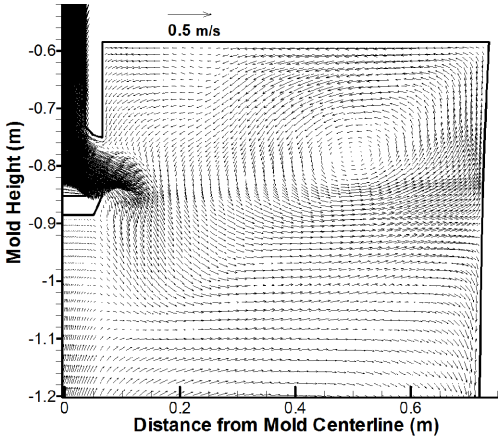

(d) Time = 2.6 sec

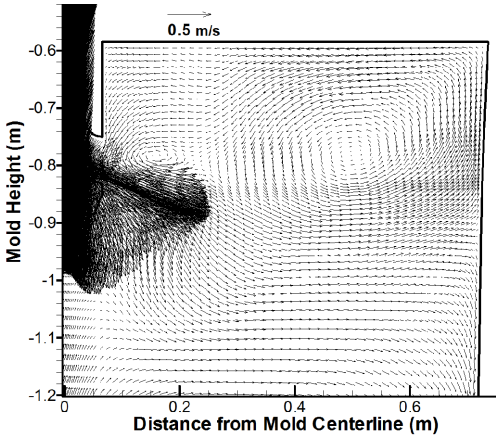

(e) Time = 3.0 sec

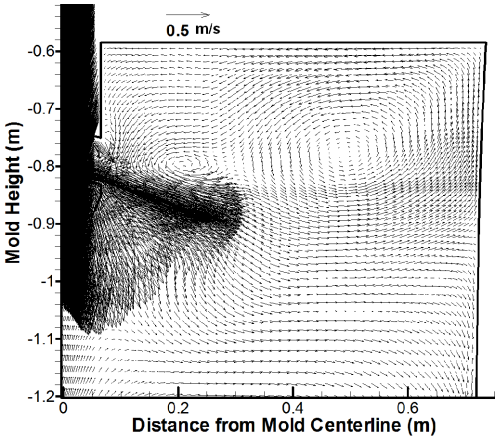

(f) Time = 3.2 sec

Figure 20. Evolution of liquid steel flow pattern during the transient event

REFERENCES

1. Hibbeler, L.C., and B.G. Thomas, "Mold Flux Entrainment Mechanisms", BAC 2010, Fourth Baosteel Biennial Conference Proceedings, Shanghai, PRC, Nov. 16, 2010, pp. B83-90.
2. Thomas, B. G., "Modeling of Continuous-Casting Defects Related to Mold Fluid Flow," *Iron and Steel Technology* (AIST Transactions, 3:5), 3:7, , July 2006, pg. 128-143.

3. Thomas, B. G., “Fluid Flow in the Mold,” Chapter 14 in Making, *Shaping and Treating of Steel*, 11th Edition, Vol. 5, Casting Volume, A. Cramb, ed., AISE Steel Foundation, Pittsburgh, PA, Oct., 2003, 14.1-14.41.
4. X. Huang and B.G. Thomas, “Modeling of Transient Flow Phenomena in Continuous Casting of Steel.” *Canadian Metallurgical Quarterly*, Vol. 37, No. 304, 1998, pg. 197-212.
5. B.G. Thomas and X. Huang, "Simulation of Argon Gas Flow Effects in a Continuous Slab Caster." *Metallurgical and Materials Transactions B*, Vol. 25B, No. 4, (August), 1994, pg. 527-547.
6. Pável Ramírez-López, R D Morales et.al., “Structure of Turbulent Flow in a Slab Mold.” *Metallurgical and Materials Transactions B,* Vol. 36B, No. 6, (Dec.), 2005, pg. 787-800.
7. R. Chaudhary, G. Lee, B.G. Thomas and S. Kim, “Transient Mold Fluid Flow with Well- and Mountain-Bottom Nozzles in Continuous Casting of Steel.” *Metallurgical and Materials Transactions B,* Vol. 39B, No. 6, Dec, 2008, pg. 870-884.
8. Q. Yuan, S. Sivaramakrishnan, S.P. Vanka, and B.G. Thomas, "Computational and Experimental Study of Turbulent Flow in a 0.4-Scale Water Model of a Continuous Steel Caster", Metallurgical and Materials Transactions B, Vol. 35B, No. 5, Oct., 2004, pg. 967-982.
9. Y. Wang and L. Zhang, “Study on Transient Fluid Flow Phenomena during Continuous Casting: Part II – Cast Speed Change, Temperature Fluctuation, and Steel Grade Mixing,” *ISIJ International*, Vol.50, No.12, 2010, pg.1783-1791.
10. E.M. Dillon, M. Sohm and D. Peters, “Validating and Identifying Continuous Casting Events Using Downstream Feedback from Automated Surface Intelligence Systems (ASIS).” *AISTech 2009 Proc., Vol(II),* pg. 523-532.
11. M.M. Yavuz and J. Sengupta, “Nozzle Design for ArcelorMittal Dofasco’s No. 1 Continuous Caster for Minimizing Sliver Defects.” *AISTech 2010 Proc., Vol(II),* pg. 41-52
12. H. Bai and B.G. Thomas, “Turbulent Flow of Liquid Steel and Argon Bubbles in Slide-Gate Tundish Nozzles, Part I: Model Development and Validation.” *Metallurgical and Materials Transactions B*, 2001, Vol. 32B, No. 2, pg. 253-267.
13. H. Bai and B.G. Thomas, “Turbulent Flow of Liquid Steel and Argon Bubbles in Slide-Gate Tundish Nozzles, Part II: Effect of Operation Conditions and Nozzle Design.” *Metallurgical and Materials Transactions B*, 2001, Vol. 32B, No. 2, pg. 269-284.
14. B. Rietow and B.G. Thomas, “Using Nail Board Experiments to Quantify Surface Velocity in the CC Mold.” *AISTech 2008 Steelmaking Conference Proc.*, (Pittsburgh, PA, May 5-8, 2008).
15. B. Rietow, *“*Investigations to Improve Product Cleanliness during the Casting of Steel Ingots.” 2007, University of Illinois at Urbana-Champaign: Urbana, IL.
16. J. Kubota, et al., “Steel Flow Control in Continuous Caster Mold by Traveling Magnetic Field,” *NKK Tech. Rev.*. 2001. pg. 1-9.
17. R. Liu, J. Sengupta, et.al. “Measurement of Molten Steel Surface Velocity with SVC and Nail Dipping during Continuous Casting Process.” *TMS 2011* (San Diego, CA, Mar 1)
18. P.H. Dauby, W.H. Emling, and R. Sobolewski, “Lubrication in the Mold: A Multiple Variable System.” *Ironmaker and Steelmaker*, 1986. 13(Feb): pg. 28-36.
19. K. Cukierski and B.G. Thomas, “Flow Control with Local Electromagnetic Braking in Continuous Casting of Steel Slabs.” *Metallurgical and Materials Transactions* 39B:1 (2008), pg. 94-107.
20. H. Bai, and B.G. Thomas, "Effects of Clogging, Argon Injection and Continuous Casting Conditions on Flow and Air Aspiration in Submerged Entry Nozzles", *Metallurgical and Materials Transactions B*, Vol. 32B, No. 4, (August), 2001, pg. 707-722.
21. D. Creech, "Computational Modeling of Multiphase Turbulent Fluid Flow and Heat Transfer in the Continuous Slab Casting Mold." MS Thesis, University of Illinois, 1999.